



Integrating Electrical Resistivity Tomography Techniques, Field Observations, and Numerical Simulations to Investigate Dynamics of Submarine Groundwater Discharge of the Taoyuan Tableland, Taiwan

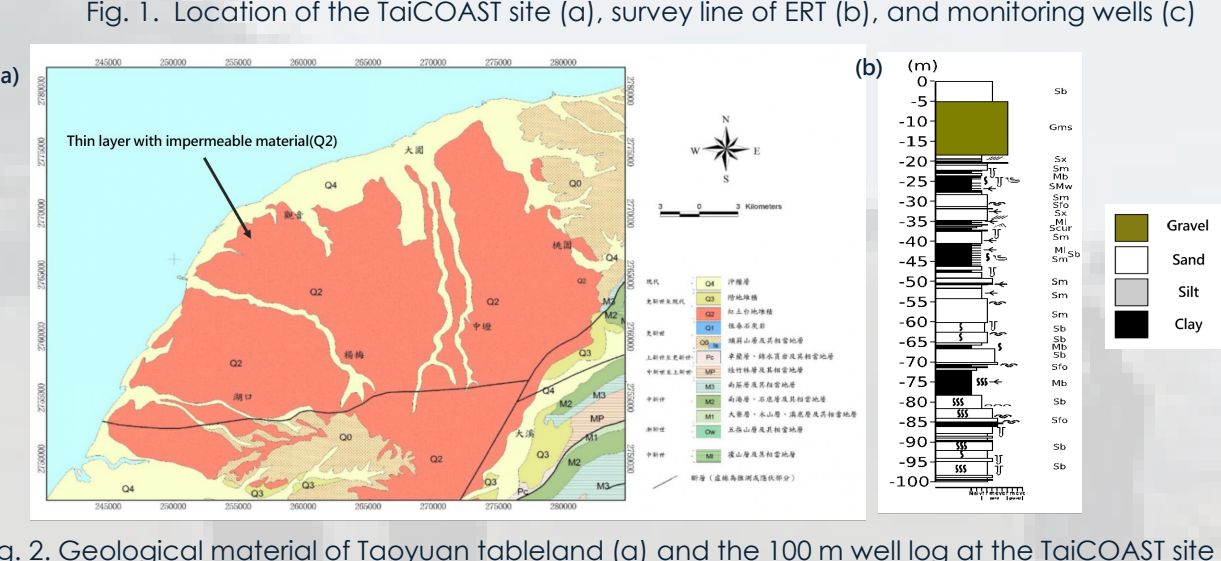
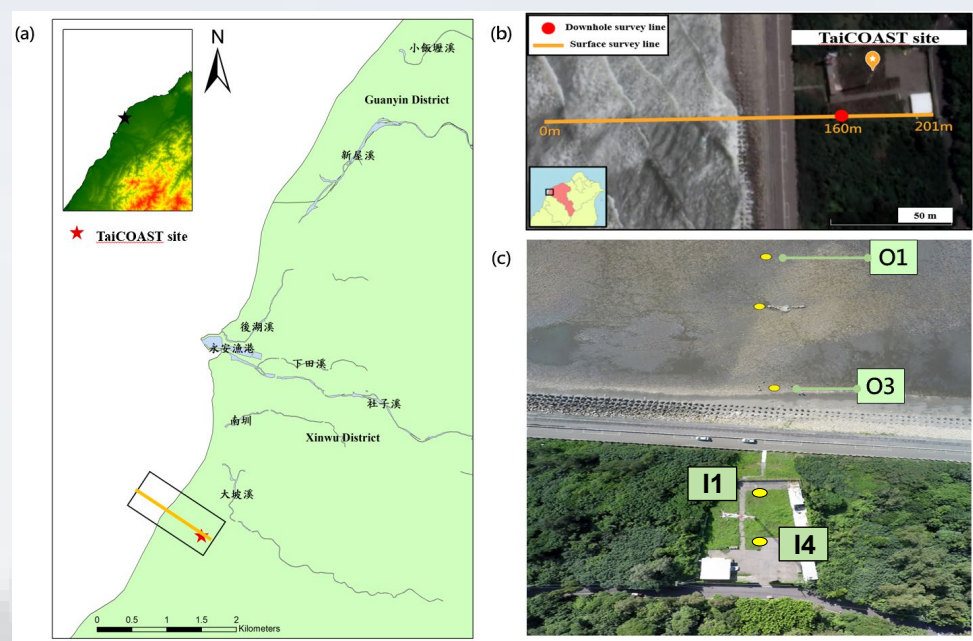
Ming-Hsu Li*, Wen-Yu Chiou, and Chien-Chih Chen
National Central University, Taoyuan, Taiwan

Abstract

Submarine groundwater discharge (SGD) dynamics are complicated and intercorrelated with hydrogeological characteristics, such as tidal variations, aquifer hydrodynamics, aquifer-sea interactions, and human activities. In this study, we aim to quantify the SGD potentials along the Taoyuan coastlines by integrating various techniques including electrical resistivity tomography (ERT), observations of water quality and water table variations, and coupled density-dependent subsurface flow and transport simulations. With a coastline length of 40 Km and an aquifer depth of 100 m, we found more than 0.5 Mt/day of freshwater is estimated to discharge into the sea. Future studies are needed to validate the feasible SGD amount to enhance coastal water resilience.

Study Area

- The surface of the Taoyuan plateau is covered by laterite, sand, and clay.
- The total length of the Taoyuan coastline is approximately 46 kilometers.
- The aquifer consists of gravel and coarse sand may be confined by an impermeable thin clay layer at the shallow depth.



Methods

Groundwater Level, Salinity, and Temperature Observations

- The CT2X Sensor (Seametric): providing observations of salinity, temperature, conductivity, solubility, and water pressure and installed at I1, I4, O1, O3 wells with different depth (Fig. 1(c))

ERT (Electrical Resistivity Tomography)

- The ERT provides high-resolution apparent resistivity data that can be transformed to salinity using an empirical formula.

Transformation from resistivity to salinity

Archie's law (Archie, 1942)

$$\rho_f = \rho_m \phi^m$$

Practical Salinity Scale (Lewis and Perkin, 1978)

$$S = a_0 + a_1 R^2 + a_2 R + a_3 R^3 + a_4 R^2 + a_5 R^5 + \Delta S$$

$$R = R_t \cdot R_p \cdot r_t = \frac{C(S, T, P)}{C(35, 15, 0)}$$

$$C(S, T, P) = \frac{1}{\rho_f} * 10^4$$

ρ_m =measured apparent resistivity (Ω/m) ; ρ_f =pore fluid resistivity (Ω/m) ; ϕ =porosity ; m =cementation coefficient ($=2$) ; S =Salinity (psu) ; T =Temperature ($^\circ\text{C}$) ; $C(35, 15, 0)$ =standard seawater conductivity ($\sim 4294 \mu\text{s/cm}$)

Coupled density-dependent subsurface flow and transport simulation (HYDROGEOCHEM 4.2, Yeh et al. 2018)

Flow equation

$$\rho_0 F \frac{\partial h}{\partial t} = \nabla \left[K \cdot (\nabla h + \frac{\rho}{\rho_0} \nabla z) \right] + \rho^* q - \frac{\partial (\theta C_j)}{\partial t} + V \cdot \nabla C_j - \nabla (\theta D \cdot \nabla C_j) = \theta r_j + M_j - Q C_j, j \in N$$

Transport equation

ρ =fluid density with dissolved chemical concentrations (M/L^3) ; ρ_0 =referenced fluid density at zero chemical concentrations (M/L^3) ; F =storage coefficient($=\rho$) or withdrawal ($=\rho$) ; h =water head (L) ; K =potential head (L) ; t =time (T) ; q =source or sink representing the artificial injection or withdrawal of fluid ($[\text{L}/\text{L}^3/\text{T}]$) ; V =transporting velocity relative to the solid of the species (L/T) ; M =external source / sink rate of the j -th species per unit medium volume ($[\text{M/L}^3/\text{T}]$) ; θr_j =production rate of the j -th species per unit medium volume due to all chemical reactions ($[\text{M/L}^3/\text{T}]$)

Hydrogeological conceptual model and Flow/Transport parameters

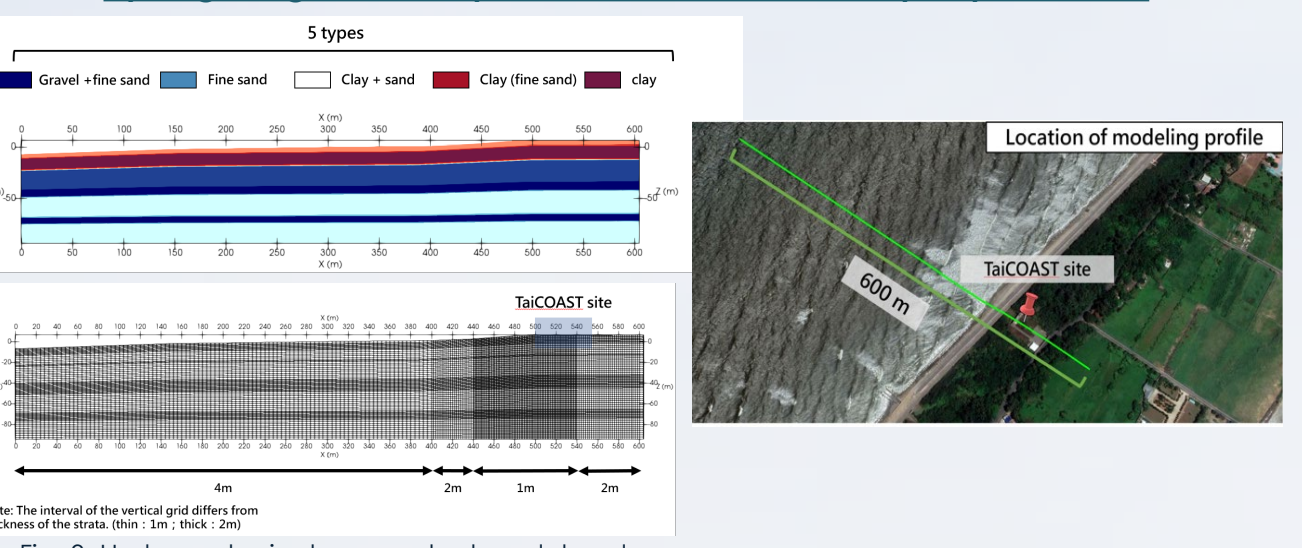


Fig. 3. Hydrogeological conceptual model and simulation grids

Table 2. Transport parameters

Material type	Porosity	K_x (m/day)	K_z (m/day)	a_1 (m)	a_5 (m)	Temperature / Pressure Setting	
						Temperature (K)	Pressure (atm)
1	0.43	3.0	1.0				
2	0.4	1.5E-01	5.0E-02				
3	0.38	7.5E-02	2.5E-02	5.00E+00	5.00E-01		
4	0.36	1.8E-02	6.0E-03				
5	0.35	7.5E-03	2.5E-03				

Boundary Conditions

B.C for flow simulation:

- Dirichlet B.C. : ABD, EF

$$h(x_b, z_b) = \begin{cases} z & z \geq b \\ 1.0245 \cdot b - 0.0245 \cdot z, & z < b \text{ at } B_d \end{cases}$$

$$C(x_b, z_b) = \begin{cases} 1.7 \cdot 10^{-3} (\text{mol/L}), & \text{for green line of } B_d \\ 3 \cdot 10^{-3} (\text{mol/L}), & \text{for yellow line of } B_d \end{cases}$$

- Variable B.C. : ABC (low tide), ABD (high tide)

$$C(x_b, z_b) = 5.5 \cdot 10^{-1} (\text{mol/L}) \text{ at } B_v$$

h_i =total head of the i -th node (L) ; C_i =salinity of the i -th node (mol/L) ; z =elevation (L) ; b =sea level (L) ; B_d =Dirichlet Boundary ; B_v =Variable Boundary

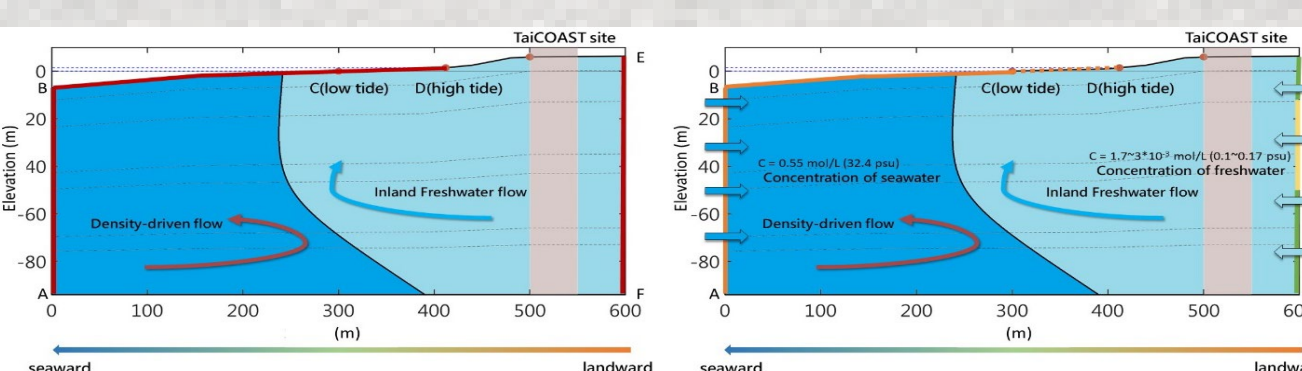


Fig. 4. Conceptual flow pattern (a) and BCs for transport simulation (b)

Conclusions

- The surface clay layer plays an important role in retarding seawater intrusion from the inundated infiltration and in supporting the fresh groundwater outflow from the tableland into the intertidal subsurface.
- The salinity from the well at the coastline is less than 0.3 PSU, considering freshwater, at a depth of 100 m with persistent strong seaward discharge throughout tidal cycles.
- The out-of-phase patterns between salinity and GWL cycles at the coastal wells, unlike the on-phase results at wells in the intertidal zones, are attributed to the slightly higher salinity in the shallow aquifer from tableland discharge possibly due to human activities.
- Although the salinity distributions retrieved by the ERT provide the salinity evolution of intertidal subsurface during tidal cycles, the values of ERT salinity are roughly one order higher than those from observations and simulations.
- More than 0.5 Mt/day SGD freshwater is estimated to discharge seaward under the sea floor based on the simulated flow velocity of about 0.15 m/day.

Acknowledgment:

This study is supported by the National Science and Technology Council with projects (112-2621-M008-003 and 111-2116-M008-018) through the National Central University.

Results

Groundwater levels, salinity, and temperature observations

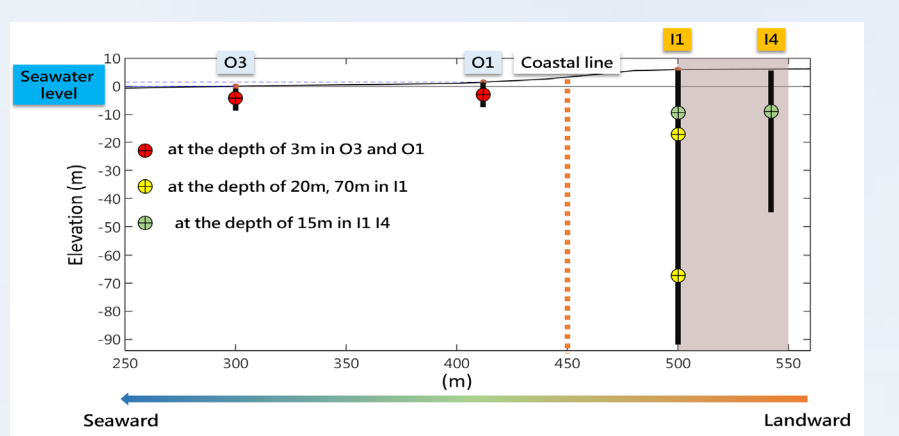


Fig. 5. Locations and depths of groundwater observations

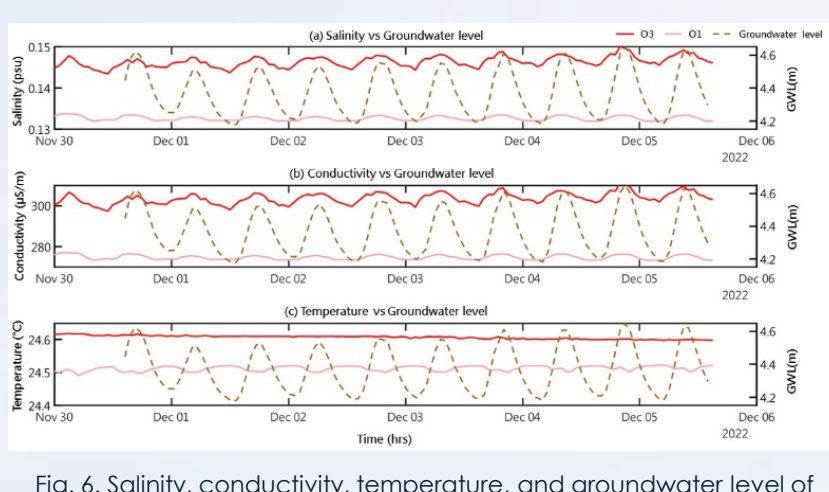


Fig. 6. Salinity, conductivity, temperature, and groundwater level of O3 and O1 at the depth of 3 m

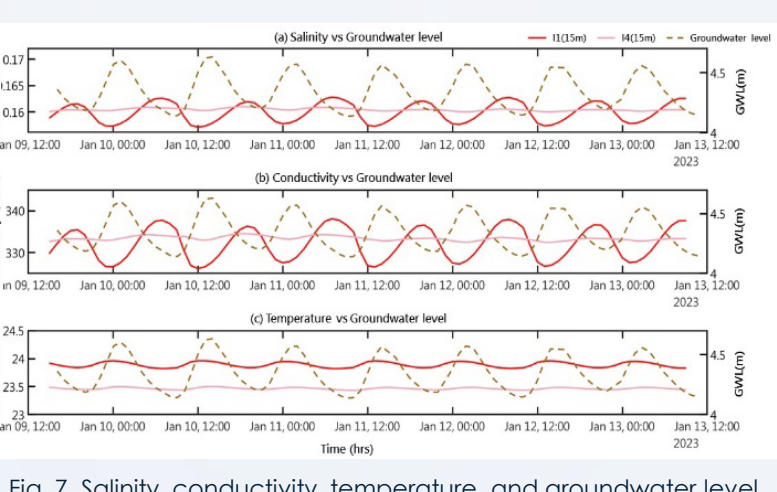


Fig. 7. Salinity, conductivity, temperature, and groundwater level of I1 and I4 at the depth of 15 m

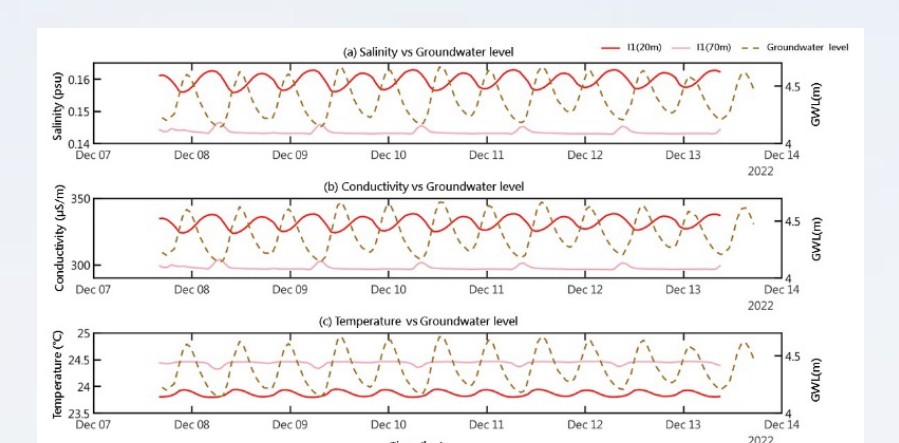


Fig. 8. Salinity, conductivity, temperature, and groundwater level of I1 at the depth of 20m and 70m

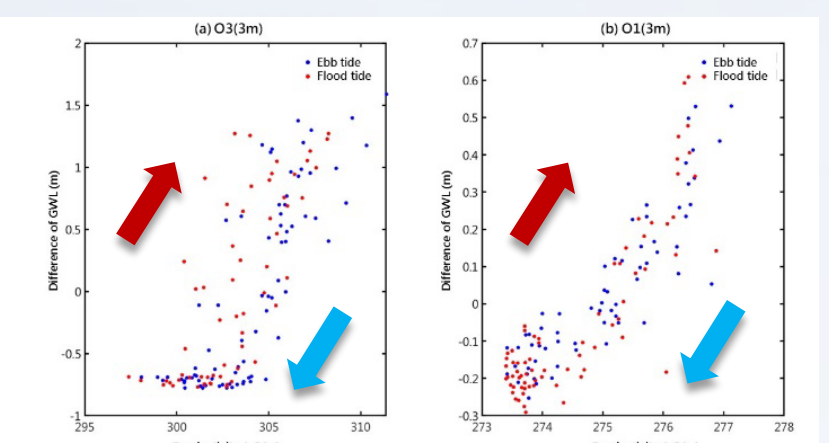


Fig. 9. Differences of GWL vs. conductivity of O3 and O1 at the depth of 3 m during ebb and flood tides

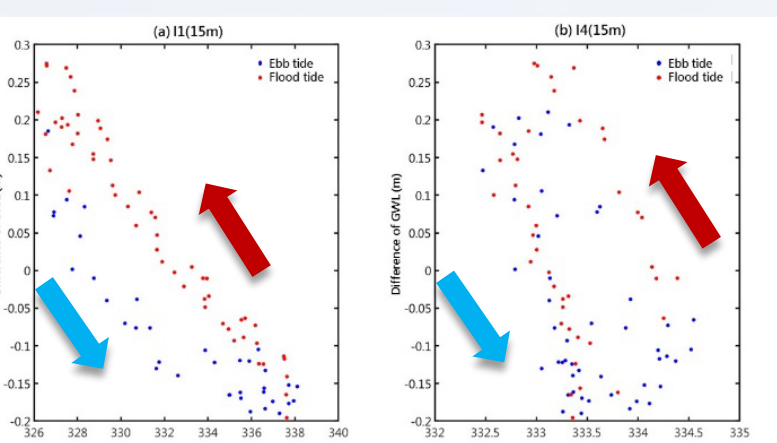


Fig. 10. Differences of GWL vs. conductivity of I1 and I4 at the depth of 15 m during ebb and flood tides

ERT (Electrical Resistivity Tomography)

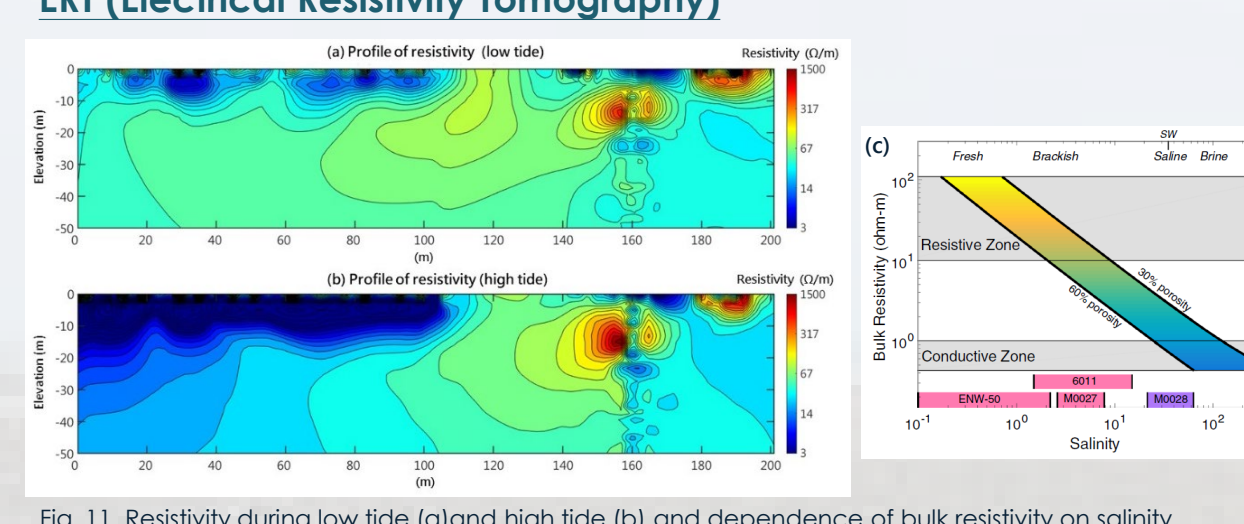


Fig. 11. Resistivity during low tide (a) and high tide (b) and dependence of bulk resistivity on salinity (Gustafson et al., 2019) (c)

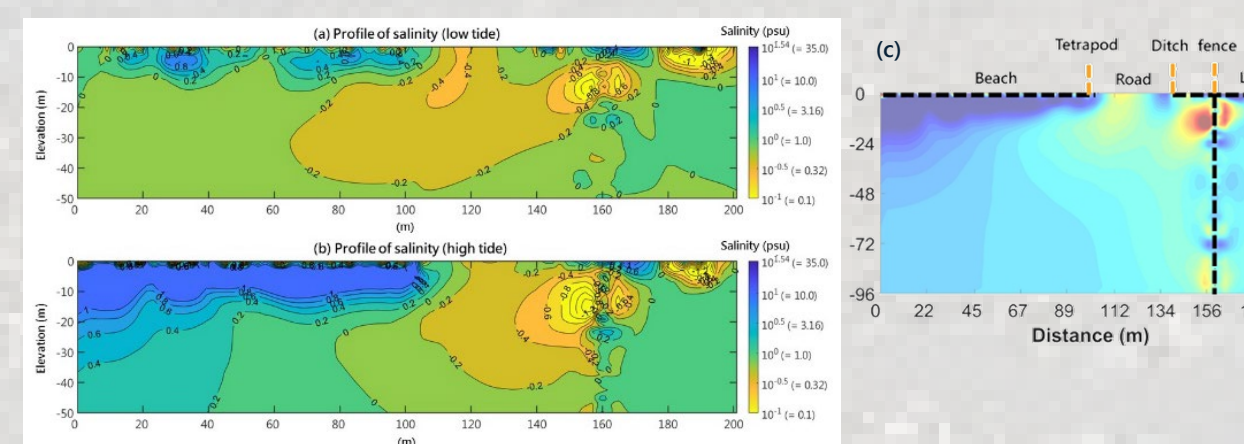


Fig. 12. Salinity during low tide (a) and high tide (b) and locations of corresponding facilities (c)

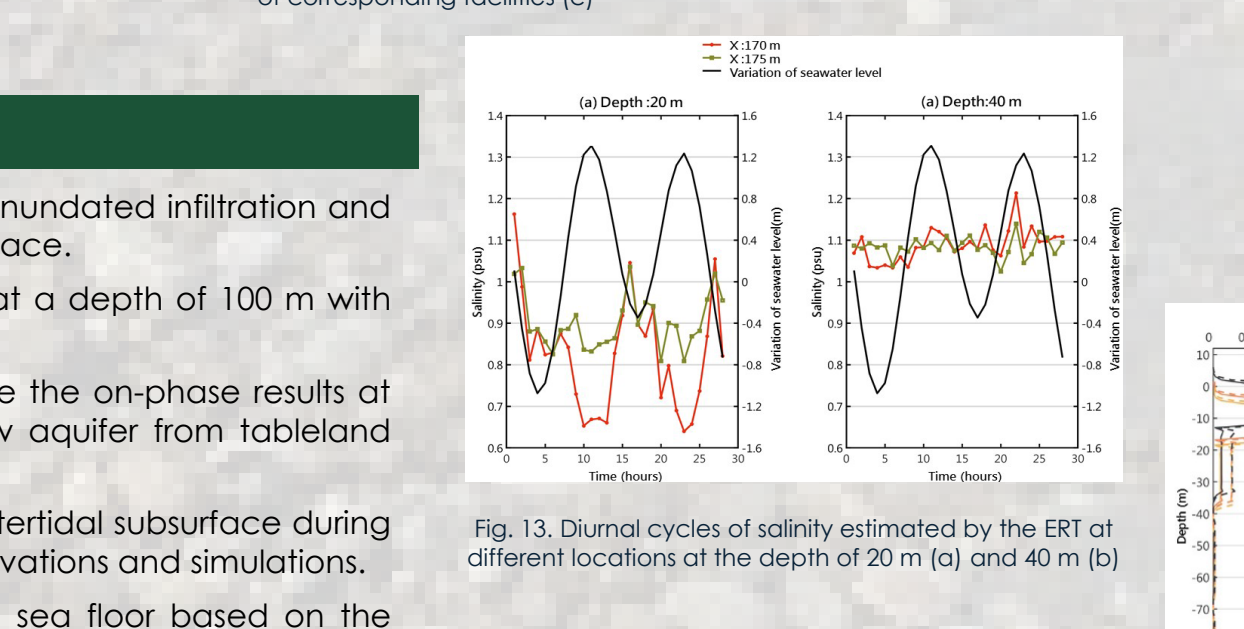


Fig. 13. Diurnal cycles of salinity estimated by the ERT at different locations at the depth of 20 m (a) and 40 m (b)

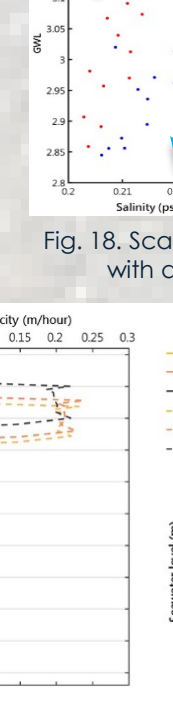


Fig. 14. Simulations of salinity and flow fields with a clay layer during low (a) and high tide (b)

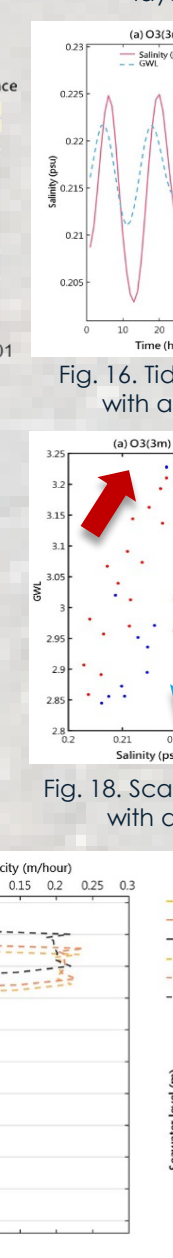


Fig. 15. Simulations of salinity profile and flow fields without a clay layer during low (a) and high tide (b)

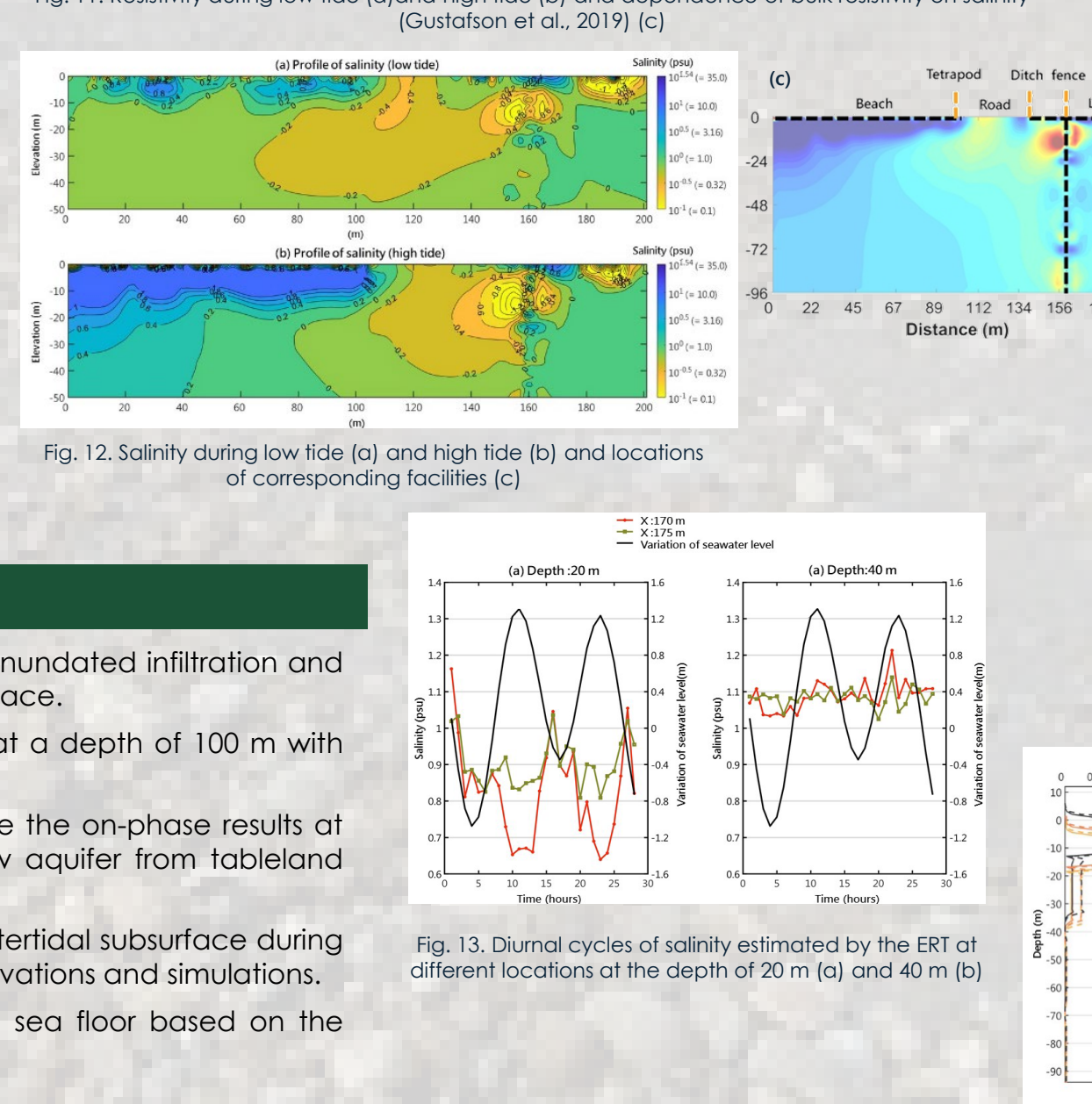


Fig. 16. Tidal cycles of salinity and groundwater level with a clay layer at O3 (a), O1 (b), and I1 (c)

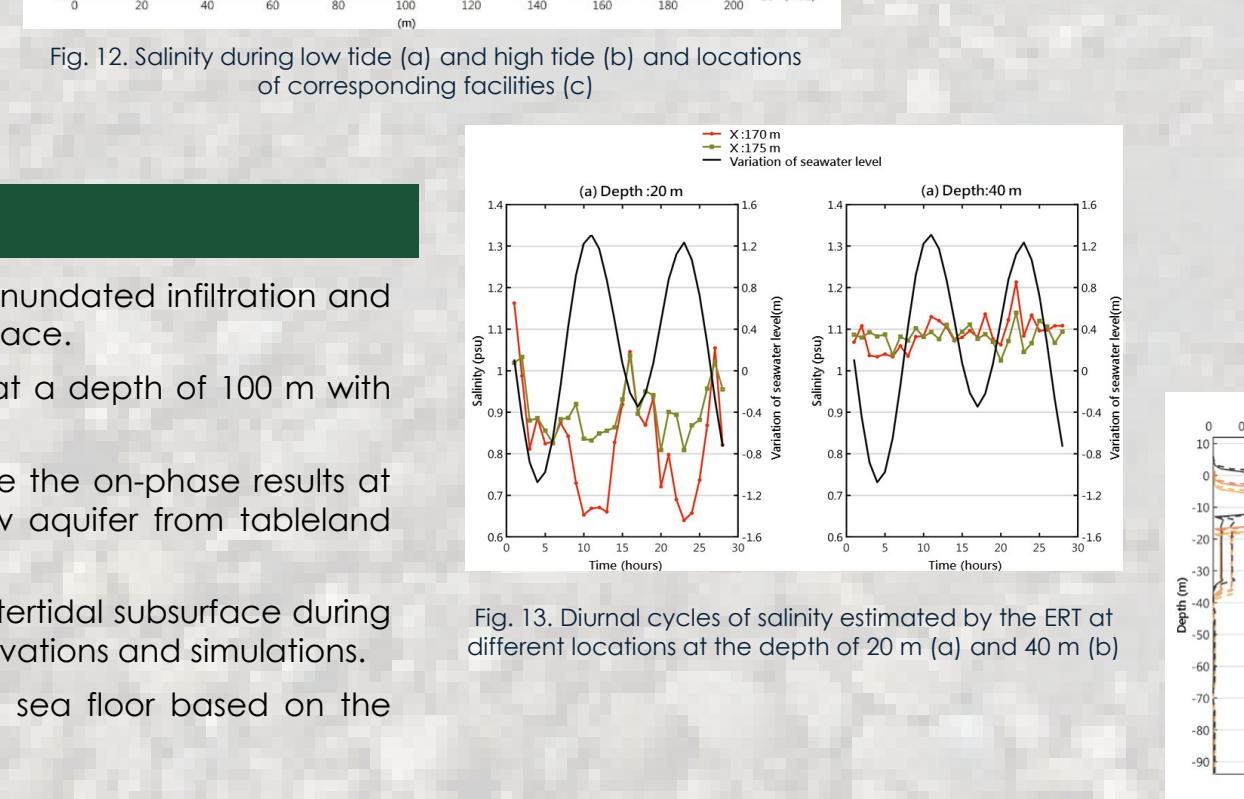


Fig. 17. Tidal cycles of salinity and groundwater level without a clay layer at O3 (a), O1 (b), and I1 (c)

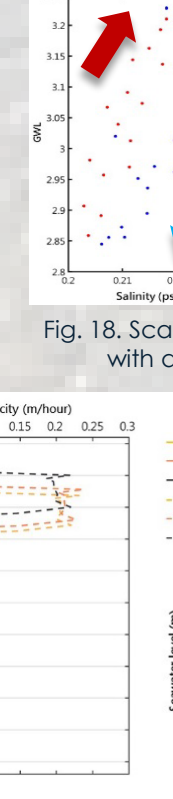


Fig. 18. Scatter plot of groundwater level and salinity with a clay layer at O3 (a), O1 (b), and I1 (c)

